ELSEVIER

Chemical Geology 244 (2007) 248–262

CHEMICAL GEOLOGY
INCLUDING ISOTOPE GEOSCIENCE

www.elsevier.com/locate/chemgeo

An accurate model to predict the thermodynamic stability of methane hydrate and methane solubility in marine environments

Rui Sun [1], Zhenhao Duan *

State Key Laboratory of Lithospheric Evolution, Institute of Geology and Geophysics, Chinese Academy of Sciences, Beijing, 100029, China

Received 24 November 2006; received in revised form 15 June 2007; accepted 16 June 2007

Editor: D. Rickard

Abstract

An accurate thermodynamic model is proposed to predict the thermodynamic stability of methane hydrate in marine environments and methane concentration needed to form hydrate in the absence of gas phase. Taking into account the effect of capillary force and salinity on chemical potential of CH_4 and H_2O, this study extends the Van der Waals–Platteeuw model and our approach to calculate the Langmuir constant from angle-dependent ab initio intermolecular potentials to marine environments. The Gibbs–Thomson equation with correct parameters for hydrate–water interface is used to account for the capillary effect of porous sediments. The Pitzer model is used to calculate the activity coefficients of H_2O and CH_4 in methane–seawater system. Comparison with the experimental data shows that this model can predict the equilibrium P–T condition of CH_4 hydrate in porous media and predict CH_4 solubility at hydrate–water equilibrium with high accuracy. The prediction of this model shows that CH_4 solubility in liquid phase at hydrate–liquid equilibrium will be reduced by increasing salinity, but it will be increased by reducing pore sizes of porous sediments. Online calculations of the P–T condition for the formation of methane hydrate and the methane solubility at a given salinity and pore sizes of sediments is made available on: www.geochem-model.org/models.htm.

Keywords: Methane hydrate; Model; Solubility; Marine sediments; Thermodynamic stability; Seawater

1. Introduction

Gas hydrates are non-stoichiometric crystalline compounds that consist of a hydrogen-bonded network of host water molecules and enclathrated guest molecules. Massive gas hydrates existed in the permafrost zone and in the seafloor sediments, containing mostly methane, are considered as a future energy source (Sloan, 1998). Release of large volumes of methane from hydrate into the ocean and atmosphere could contribute significantly to global warming (Dickens, 2003) and trigger submarine landslides (Xu and Germanovich, 2006).

Methane hydrate is stable at low temperatures and high pressures. Fig. 1 shows the phase assemblage of CH_4–H_2O binary system. Q_1 is the quadruple invariant point where CH_4 hydrate (H), ice (I), water-rich liquid (L), CH_4-rich vapor (V) phases coexist. Line AQ_1B represents the P–T condition for H–I–V equilibrium or H–L–V three-phase equilibrium, which marks the

* Corresponding author. Tel.: +86 10 62007447; fax: +86 10 62010846.
E-mail address: duanzhenhao@yahoo.com (Z. Duan).
[1] Present address. CREGU et UMR G2R(7566), Faculté des Sciences, Université Henri Poincaré, Nancy 1, BP 23, 54500 Vandoeuvre-lès-Nancy, France.

0009-2541/$ - see front matter © 2007 Elsevier B.V. All rights reserved.
doi:10.1016/j.chemgeo.2007.06.021

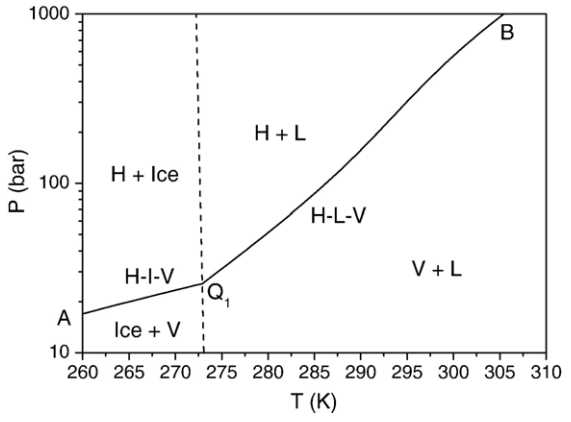

Fig. 1. P–T phase diagram of the CH_4–H_2O binary system at low temperatures.

stable boundary of methane hydrate. According to phase rule, two phases can coexist in the regions above and below the line AQ_1B. The region where CH_4 hydrate can exist stably. In the region below the triple phase line, CH_4-rich vapor coexists with liquid water or ice.

In marine sediments, methane hydrate is restricted to locations where the required pressure and temperature conditions are met and where the abundance of methane is sufficient to exceed the local solubility (Kvenvolden, 1988). It is well accepted that the P–T condition at the base of hydrate stability zones match the P–T condition for three-phase equilibrium between water, hydrate and free gas (Henry et al., 1999; Davie et al., 2004). Within the hydrate stability zone, methane hydrate phase coexists with liquid water phase. In this two-phase region, any free gas will be completely incorporated into the hydrate structure due to the abundance of water (Handa, 1990; Zatsepina and Buffett, 1997) except in fault zones where gas passes through the entire hydrate stability zone and bubbles into the overlying ocean (Kleinberg et al., 2003; Cathles and Chen, 2004). The solubility of methane in water defines the minimum methane concentration needed to form hydrate. Understanding the P–T condition for H–L–V equilibrium and methane solubility at hydrate–liquid equilibrium (H–L equilibrium) in marine sediments is important for exploring and exploiting methane hydrate resource, investigating the formation kinetics of hydrates (Servio and Englezos, 2002), and modeling the geochemical processes of hydrates in various geological settings (Zhang and Xu, 2003).

Many thermodynamic models for calculating phase equilibria of gas hydrates have been proposed since the prominent work of Van der Waals and Platteeuw (1959). However, most of the previous works dealt with the three-phase equilibrium of gas hydrates in bulk system, such as the work of Parrish and Prausnitz (1972), Ng and Robinson (1976), Englezos and Bishnoi (1988), Tohidi et al. (1995), Chen and Guo (1998), Ballard and Sloan (2002), and Lee and Holder (2002). We also published thermodynamic models to predict the three-phase equilibrium of CH_4 hydrate and CO_2 hydrate in bulk water–gas–salt system (Sun and Duan, 2005; Duan and Sun, 2006). Until now, only a few theoretical studies dealt with hydrate–liquid two-phase equilibrium in bulk or in porous media and three-phase equilibrium in porous media. Applying Gibbs–Thomson equation to account for the capillary effect arising from the small pore size, Clennell et al. (1999) and Henry et al. (1999) developed a thermodynamic model to predict the three-phase equilibrium of CH_4 hydrate in marine sediments. Later, Klauda and Sandler (2001, 2003) proposed an improved model and predicted the distribution of methane hydrate in ocean sediment. However, these models used incorrect interface parameters (Llamedo et al., 2004). The shape factor (curvature) of hydrate–liquid interface assumed by them corresponds not to hydrate equilibrium, but to hydrate growth. Therefore, these models overestimate the inhibition effect of the capillary force on H–L–V equilibrium. In general, there is still no model that can predict the P–T condition for H–L–V equilibrium of methane hydrate in marine sediments accurately to date.

Handa (1990), Zatsepina and Buffett (1997, 1998), Tishchenko et al. (2005) investigated the effect of temperature, pressure, and salinity on CH_4 solubility at hydrate–liquid. Clennell et al. (1999) and Henry et al. (1999) examined the capillary effect on CH_4 solubility at H–L equilibrium. Although these models can predict the variation of methane solubility with temperature, pressure and salinity at H–L equilibrium, there is substantial room for improvements. The model of Zatsepina and Buffett (1997, 1998) underestimated CH_4 solubility in water and underestimated the salting-out effect of electrolyte on CH_4 solubility both at V–L equilibrium and at H–L equilibrium. Hashemi et al. (2006) improved the model of Zatsepina and Buffett (1997) so that their model can predict CH_4 solubility in pure water at H–L equilibrium with high accuracy. The model of Handa (1990) and Tishchenko et al. (2005) can predict CH_4 solubility in pure water and in seawater at H–L equilibrium accurately. However, Handa (1990) made an unreasonable assumption that the ratio of cage occupancies along three-phase equilibrium is constant at various temperatures so that their model cannot predict the cage occupancy of methane hydrate well. Both experimental and theoretical studies (Sum et al., 1997;

Sloan, 1998; Jager, 2001) show that the ratio of cage occupancies varies with temperature and pressure. Tishchenko et al. (2005) used an empirical formula to calculate three-phase equilibrium of methane hydrate in pure water so that their model has no function to predict the cage occupancy.

The purpose of this study is to develop an accurate model to predict the P–T condition for three-phase equilibrium (H–L–V equilibrium) and CH_4 solubility in liquid at two-phase equilibrium (H–L equilibrium) in marine environments by taking into account the effect of temperature, pressure, salinity and capillary force together. Van der Waals–Platteeuw basic hydrate model is used to describe the chemical potential of hydrate phase. The Langmuir constants are calculated from angle-dependent ab initio intermolecular potentials as our previous work (Sun and Duan, 2005). The fugacity of gas methane is calculated from equation of state developed by Duan et al. (1992a) while the fugacity of methane dissolved in aqueous solution at H–L equilibrium where CH_4 gas phase does not exist is calculated with Poynting correction. The effect of salts and porous sediments on H–L–V equilibrium and H–L equilibrium are addressed based on accurate thermodynamic methods. The next section will introduce the thermodynamic model proposed by this study. Section 3 compares the experimental data with predictions of this model for the thermodynamic stability of methane hydrate and CH_4 solubility in aqueous solution. Finally, some conclusions are drawn.

2. Thermodynamic model of gas hydrates

2.1. General thermodynamic equations

At phase equilibrium, the fugacities or chemical potentials of species in the various phases must be equal. For water, the following equation must be satisfied

$$\Delta\mu_w^H = \mu_w^\beta - \mu_w^H = \mu_w^\beta - \mu_w^L = \Delta\mu_w^L \quad (1)$$

where μ_w^H is the chemical potential of water in hydrate, μ_w^L is the chemical potential of water in liquid phase, and μ_w^β is the chemical potential of water in the hypothetical empty hydrate lattice at the same temperature and pressure.

$\Delta\mu_w^H$ is calculated from the statistical mechanics model proposed by Van der Waals and Platteeuw (1959)

$$\Delta\mu_w^H(T,P) = -RT\sum_{i=1}^{2} v_i \ln\left(1-\sum_{j=1}^{N_C}\theta_{ij}\right) \quad (2)$$

where v_i is the number of i-type cages (also called "cavities") per water molecule, θ_{ij} is the fractional occupancy of i-type cavities with j-type guest molecules. For sI hydrate, the number of small cavities, v_1, equals to 1/23, the number of large cages, v_2, equals to 3/23. The expression for θ_{ij} is

$$\theta_{ij} = C_{ij} f_j \Big/ \left(1+\sum_{j=1}^{N_C} C_{ij} f_j\right) \quad (3)$$

where C_{ij} is the temperature-dependent Langmuir constant of gas component j in i-type cavity, and f_j is the fugacity of gas component j in hydrate phase.

The Langmuir constant is the key parameter of van der Waals–Platteeuw model, which depends on the interaction potential between guest molecule and water molecules. Most of the previous hydrate models calculated the Langmuir constant from the Kihara potential model with parameters determined from phase equilibrium data of gas hydrates. We presented a new method to calculate C_{ij} from angle-dependent ab initio intermolecular potentials recently (Sun and Duan 2005). This method is used in this work. Appendix A gives a detailed description of the calculation of the Langmuir constants.

Another important aspect is to calculate the fugacity of gas component from accurate thermodynamic model. At hydrate–liquid water-vapor three-phase equilibrium, the fugacity of CH_4 in hydrate phase is equal to that in aqueous solution and that in vapor phase

$$f_{CH_4}^H = f_{CH_4}^L = f_{CH_4}^V \quad (4)$$

where the superscript H means hydrate phase, L means liquid phase, V means vapor phase. Numerous equations of state (EOS) were designed to predict the thermodynamic properties of pure gas or gas mixtures. This study adopted the equation of state developed by Duan et al. (1992a) to calculate the fugacity of CH_4 in vapor phase.

At two-phase hydrate–liquid water equilibrium, vapor CH_4 phase is absent. So we cannot calculate f_{CH_4} by using EOS designed for CH_4 gas. There are few equations of state which can calculate the fugacity of CH_4 in aqueous phase which does not coexist with vapor phase. This study use a rigorous thermodynamic equation—Poynting correction (Prausnitz et al., 1986; Holder et al., 2001) to calculate the fugacity of CH_4 in single liquid phase

$$f_{CH_4}^L(T,P,x_{CH_4}) = f_{CH_4}^{sat}\exp\left[\int_{P^{sat}}^{P}\frac{\overline{V}_{CH_4}dP}{RT}\right] \quad (5)$$

where P^{sat} is defined as the pressure required to obtain a given solubility, x_{CH_4}, $f_{CH_4}^{sat}$ represents the fugacity of

CH_4 at P^{sat}, $\overline{V}_{CH_4}$ means the partial molar volume of CH_4 in aqueous solution.

Eq. (5) gives the relationship between f_{CH_4} in single liquid phase and f_{CH_4} at V–L phase boundary. At P^{sat}, CH_4-rich vapor coexists with H_2O-rich liquid. Thus, f_{CH_4} can be calculated from EOS designed for gas phase (i.e. the EOS of Duan et al. (1992a)). Methane solubility at V–L equilibrium and H–L–V equilibrium and $\overline{V}_{CH_4}$ are calculated from the solubility model of Duan and Mao (2006).

$\Delta\mu_w^L$ is calculated from the expression proposed by Holder et al. (1980)

$$\frac{\Delta\mu_w^L(T,P)}{RT} = \frac{\Delta\mu_w^0(T_0,0)}{RT_0} - \int_{T_0}^{T}\left(\frac{\Delta h_w^{\beta-L}}{RT^2}\right)dT + \int_0^P\left(\frac{\Delta V_w^{\beta-L}}{RT}\right)dP - \ln a_w \quad (6)$$

$$\Delta h_w^{\beta-L} = \Delta h_w^0(T_0) + \Delta h_w^{\alpha-L} + \int_{T_0}^{T}\Delta C_p dT \quad (7)$$

where $\Delta\mu_w^0(T_0,0)$ is the reference chemical potential difference of water between empty hydrate phase and ice at the reference temperature, T_0, usually taken to be 273.15K, and zero pressure. $\Delta h_w^{\beta-L}$ and $\Delta V_w^{\beta-L}$ and represents the difference of enthalpy and the molar volume between hydrate and liquid water, respectively. Δh_w^0 is the difference of enthalpy between hydrate phase and ice at T_0, and ΔC_p is the difference of isobaric thermal capacity. a_w means the activity of water. The values of $\Delta\mu_w^0$ and Δh_w^0 were determined from three-phase equilibrium data of methane hydrate in CH_4–H_2O system by our previous study (Sun and Duan, 2005). The value of ΔC_p determined by Parrish and Prausnitz (1972) is adopted. Table 1 gives the values of $\Delta\mu_w^0$, Δh_w^0 and ΔC_p for sI hydrate. The molar volume of liquid water can be calculated from the EOS of Sun et al. (2003). Eq. (8) is the formula to calculate the molar volume of water in empty sI hydrate phase, V_w^β, which was also determined by our previous study.

$$V_w^\beta(T,P) = \left(11.820 + 2.217\times10^{-5}T + 2.242\times10^{-6}T^2\right)^3\frac{10^{-30}N_A}{N_w^\beta} \times \exp\left(-3.5\times10^{-4}(P-0.1) + 7.07 \times10^{-6}(P-0.1)^{1.5}\right) \quad (8)$$

where N_A is Avogadro's number, N_w^β means the number of water molecules per hydrate cell. For sI hydrate, N_w^β equals to 46. The unit of pressure in Eq. (8) is MPa, and the unit of temperature is Kelvin.

Table 1
Thermodynamic reference properties for sI hydrate: T_0=273.15K

$\Delta\mu_w^0$ (J/mol)	1202.
Δh_w^0 (J/mol)	1300.
$\Delta h_w^{\alpha-L}$ (J/mol)	−6009.5
$\Delta C_p^{\beta-L}$ (J/mol/K)	$-38.12+0.141\times(T-T_0)$
$\Delta C_p^{\beta-\alpha}$ (J/mol/K)	$0.565+0.002\times(T-T_0)$

The P–T condition for three-phase equilibrium or methane solubility at H–L two-phase equilibrium can be calculated by iteration of Eq. (1). Here we give some description of the solving procedure. In order to calculate the equilibrium pressure for H–L–V equilibrium at a given temperature T, we can guess an initial value P_1 for pressure firstly and calculate C_{ij}, $f_{CH_4}^V$, $\Delta h_w^{\beta-L}$, $\Delta V_w^{\beta-L}$ and a_w at P_1. Then we substitute them into Eqs. (2), (3) and (6) to obtain $\Delta\mu_w^H$ and $\Delta\mu_w^L$. Now, we compare the value of $\Delta\mu_w^H$ with the value of $\Delta\mu_w^L$. If the absolute difference between $\Delta\mu_w^H$ and $\Delta\mu_w^L$ is small enough (e.g. 1×10^{-2}), the pressure can be considered as the equilibrium pressure at T. Otherwise, we change the value of pressure and calculate $\Delta\mu_w^H$ and $\Delta\mu_w^L$ at new pressure. This process is repeated until we find the equilibrium pressure. The Newton Iteration Method or dichotomy can be used. The absolute difference between $\Delta\mu_w^H$ and $\Delta\mu_w^L$ is less than 1×10^{-2} is chosen as the condition for stopping iterating so that we can obtain the equilibrium pressure with deviation less than 0.1%.

For the calculation of methane solubility in aqueous solution at H–L equilibrium at a given temperature and pressure, we guess an initial value for x_{CH_4} at first and solve the saturation pressure P^{sat} corresponding to x_{CH_4} based on CH_4 solubility model by iterating. Then we calculate $f_{CH_4}^L$ in terms of Eq. (5) and substitute it into Eqs. (2) and (3) to calculate $\Delta\mu_w^H$. Finally we calculate $\Delta\mu_w^L$ based on Eq. (6) and compare it with $\Delta\mu_w^H$. If the absolute difference between $\Delta\mu_w^H$ and $\Delta\mu_w^L$ is less than 1×10^{-2}, x_{CH_4} can be considered as CH_4 solubility at H–L equilibrium. Otherwise, we change the value of x_{CH4} and repeating. It should be noticed that the method to calculate the fugacity and solubility of CH_4 at H–L–V equilibrium and V–L equilibrium is different from the method to calculate the fugacity and solubility of CH_4 at H–L equilibrium.

2.2. Influence of electrolytes

Electrolytes cannot enter the lattice of hydrates, so they do not change the chemical potential of water in hydrate phase. However, electrolytes presented in liquid phase will change the activity of water and methane in aqueous solution, thus affecting H–L–V equilibrium

and H–L equilibrium of methane hydrate. Zatsepina and Buffett (1998) adopted Aasberg–Petersen's model (Aasberg-Petersen et al., 1991) to calculate the activity coefficient of water and methane in aqueous solutions. However, Aasberg–Petersen's model underestimates the salting-out effect of electrolyte on CH_4 solubility (i.e. underestimate the activity coefficient of CH_4 in aqueous electrolyte solution) at vapor–liquid equilibrium and overestimates the activity of water at lower temperatures ($T<303$K) since its water–salt and gas–salt interaction parameters were determined from the data at higher temperatures (vapor pressure data of salt solution at 373K and gas solubility data above 323K). The experimental data indicates that the activity coefficient of dissolved methane, γ_{CH_4}, decrease with the increase of temperature from 273 to 373K. For example, the value of γ_{CH_4} at 273K and 323K in 1m NaCl solution is about 1.40 and 1.26, respectively. Clennell et al. (1999) and Henry et al. (1999) adopted methane solubility model developed by Duan et al. (1992b), which was found to underestimates the activity coefficient of CH_4 in aqueous electrolyte solution at temperatures below 303K. The underestimation was recently corrected by Duan and Mao (2006).

We adopted Pitzer model (1991) together with temperature-dependent parameters to calculate the activity of water and made progress in predicting P–T condition for H–L–V equilibrium in various electrolyte solutions (Duan and Sun, 2006). This method was followed by this study to calculate a_w in seawater. The solubility of CH_4 in aqueous solution at H–L–V equilibrium and the interaction parameters between ion and CH_4 were calculated from solubility model of Duan and Mao (2006).

The equations to calculate a_w based on Pitzer model is omitted here to keep the paper concise. The readers can find them in the paper of Duan and Sun (2006).

2.3. Effect of porous media

Naturally occurring methane hydrates are distributed in pore space of sediments. Some evidences indicate that the pore size (Ruppel, 1997; Clennell et al., 1999), the surface textures and mineral components may affect the three-phase equilibrium conditions of gas hydrates. In recent years, a lot of experiments (Handa and Stupin, 1992; Uchida et al., 1999, 2002; Seshadri et al., 2001; Smith et al., 2002a,b; Zhang et al., 2002; Seo et al., 2002a; Seo and Lee, 2003; Anderson et al., 2003a; Aladko et al., 2004) were performed to measure the H–L–V equilibrium of gas hydrates in synthetic porous media. These studies indicate that capillary force inhibits the formation of gas hydrates in narrow pores. For the effect of surface textures and mineral components on the stability of gas hydrates, there exists controversy in earlier researches. The latest experiments made by Riestenberg et al. (2003) and Uchida et al. (2004) shows that the surface textures and mineral components have little influence on the phase equilibrium of CH_4 hydrate. Thus, this model will take into account the effect of pore size on phase equilibrium of methane hydrate and ignore the effect of the surface textures and mineral components based on the studies to date.

Based on Gibbs–Thomson equation, Clennell et al. (1999) and Henry et al. (1999) proposed an equation to calculate the chemical potential difference of water arising from capillary force. Their equation was followed by other models (Clarke et al., 1999; Klauda and Sandler, 2001, 2003; Wilder et al., 2001; Seo et al., 2002a). However, it was designed for hydrate growth. Dicharry et al. (2005) proposed the equation for hydrate dissociation in porous media as following

$$\Delta\mu_w^L(\text{pore}) = \Delta\mu_w^L(\text{bulk}) + V^\beta \frac{F\sigma_{HW}\cos\alpha}{r} \quad (9)$$

where V^β is the molar volume of water in the hydrate lattice, F is the shape factor of solid–liquid interface, α is the contact angle between the solid phase and the pore wall, r means the radius of pore, σ_{HW} means the interfacial energy (interfacial tension) between hydrate phase and liquid phase.

Some assumptions should be made for Eq. (9): (1) The bulk structural properties of hydrate are retained in pore space. Seo et al. (2002a) found through NMR spectroscopy that the structure of CH_4 hydrate in silica gel pores with diameter of 6.0nm is identical with that of bulk CH_4 hydrate. Thus we can expect that Eq. (9) can work for pores with diameters greater than 6.0nm; (2) liquid water is considered as continuous phase because the silica surface is hydrophilic and the amount of water is much more than the amount of gas and the hydrate in pore space. In contrast, hydrate is non-wetting on pore walls so that $\cos\alpha$ equals to 1. There exists a bound water layer (unfrozen water layer) between hydrate and pore wall (Handa and Stupin, 1992). The thickness of the bound water layer is assumed to be 0.4nm based on the study of Schreiber et al. (2001). (3) There exists hydrate–water interface rather than hydrate–gas interface inside pores. Hydrate particles in pores contact with continuous water phase and methane gas preferentially fills the larger pores to form bulk phase since the interfacial tension between vapor CH_4 and liquid water is greater than that between hydrate and water. Therefore, this study ignores the effect of capillary force on the

chemical potential of methane at equilibrium. (4) The shape of pores and hydrate particles in pore space is cylindrical. Although the pores may have complex shape, it has been found that the cylindrical model fits well the H–L–V equilibrium data and the ice–liquid water equilibrium data in synthetic porous media. We expect the cylindrical model to represent the shape of hydrate particles in pore space within sediment matrix.

Strictly speaking, r in Eq. (9) is the radius of cylindrical hydrate particle in pores, which equals the radius of pore minus the thickness of bound water layer. This definition is used by this study. On the contrary, previous models used the radius of pore to represent r although some of them recognized the existence of bound water layer.

F and σ_{HW} are the key parameters of Eq. (9). However, various choices for these parameters exist in previous studies. The shape factor (F) of interface is equal to 1 and 2 for cylindrical hydrate particle and spherical hydrate particle, respectively. Anderson et al. (2003a) and Llamedo et al. (2004) pointed out that cylindrical shape ($F=1$) corresponds to hydrate dissociation and spherical shape ($F=2$) corresponds to hydrate growth. Due to the hysteresis for hydrate growing, the P–T condition at hydrate dissociation is a more accurate representation of the true equilibrium condition than the P–T condition at hydrate growth. Therefore, we assume F equal to 1 in this study. On the contrary, the majority of studies in modeling hydrate equilibrium in porous media incorrectly assumed F equal to 2, which leads to the overestimation of the inhibition effect of the capillary force on H–L–V equilibrium.

There is no direct measurement on the hydrate–liquid water interfacial energy available. Clennell et al. (1999) and Henry et al. (1999) assumed that the interfacial energy between hydrate and water phase, σ_{HW}, equals to that between ice and water phase, σ_{IW}. This assumption was confirmed by Zhang et al. (2002) through measurements of hydrate–ice–gas equilibrium in porous media. The majority measurements existed in literature indicate that the value of σ_{IW} at 273.15K varies from 25 to 33mJ/m^2 (Hillig, 1998; Anderson et al., 2003b). This model adopts the ice–water interface energy determined by a recent study (i.e. Hillig (1998), $\sigma_{IW}=31.7$mJ/m^2) to represent hydrate–water interface energy. Uchida et al. (2002) evaluated the methane hydrate–liquid water interfacial energy from experimental data of hydrate equilibrium in porous media. However, the value obtained by them is 17 ± 3mJ/m^2, which is about half of ice–water interfacial energy due to the assumption that the shape factor equals to 2. Assuming the shape factor equals to 1, Anderson et al. (2003b) obtained a value of 32 ± 2mJ/m^2, which is consistent with the ice–water interfacial energy.

σ_{IW} may vary with temperature, pore size (or curvature), and the salinity of aqueous solution. Tolman (1949) proposed the following equation to describe the curvature effect on interfacial energy

$$\sigma = \frac{\sigma^{\infty}}{1+\frac{2\delta}{r}} \tag{10}$$

where σ^{∞} is the interfacial energy between plane interface, δ is called Tolman length, which represents the thickness of the interfacial region.

Bogdan (1997) estimated δ for ice–liquid water interface as 0.4186nm at 273.15K. This value was adopted by this study to calculate the curvature effect on σ_{HW} ($\sigma^{\infty}_{HW}=31.7$mJ/m^2). The curvature in Eq. (10), $2/r$, which represents spherical interface, was replaced with $1/r$ since the hydrate–water interface for hydrate dissociation is cylindrical.

Several studies found that σ_{IW} decreases with the decrease in temperature in the range below 273.15K. However, we are not sure that the temperature-dependent coefficient can be extrapolated to temperatures above 273.15K and elevated pressures. Jones (1973), Hardy and Coriell (1973) measured the ice–aqueous NaCl solution interfacial energy, but the uncertainty of their measurements is large. Thus, this study neglected the temperature- and salinity-dependence of σ_{HW}.

3. Results and discussion

3.1. H–L–V equilibrium in seawater and in porous media

Sun and Duan (Sun and Duan, 2005; Duan and Sun, 2006) have demonstrated that the P–T conditions for three-phase equilibrium of methane hydrate in water and in various aqueous electrolyte solutions can be accurately predicted. Fig. 2 shows the agreement between the predictions of our model and experimental data (Dholabhai et al., 1991; Dickens and Quinby-Hunt, 1994) for three-phase equilibrium of methane hydrate in seawater. In this text, the term 'seawater' means seawater with standard sea salt composition except where there is special statement. The molality of major ions in 35wt.‰ seawater is taken from Riley and Skirrow (1975) and is listed in Table 2. We assume the molality of ions in seawater with weight percent other than 35‰ is proportional to that in 35‰ seawater. Although the experimental data on H–L–V equilibrium of CH_4 hydrate in seawater is limited to pressures below 100bar, we believe that it can be extended to higher pressures since the model can predict H–L–V

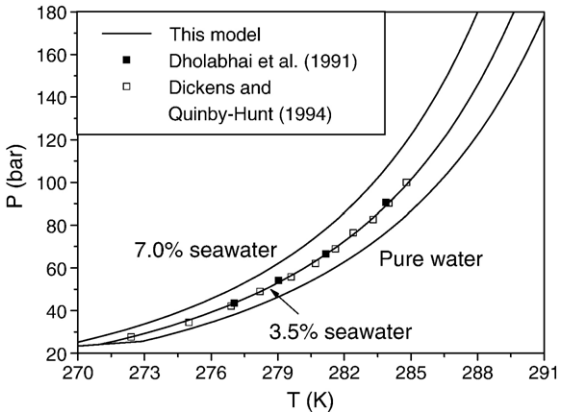

Fig. 2. The prediction of this model for three-phase (H–L–V) equilibrium of methane hydrate in seawater.

equilibrium of CH_4 hydrate in water and in aqueous NaCl solutions to pressures up to 2000bar.

Fig. 3 shows the prediction of this model for the three-phase equilibrium of methane hydrate in cylindrical pores of different sizes. Each line in Fig. 3 represents the P–T condition for three-phase equilibrium of CH_4 hydrate in pores with uniform size. The experimental data measured by Anderson et al. (2003b), Uchida et al. (2002), and Seo et al. (2002a) are shown in Fig. 3 to verify this model. It is clear that the prediction of this model agrees well with all the data of Anderson et al. (2003b), and most of the data of Uchida et al. (2002) and Seo et al. (2002a). There is an obvious discrepancy between the measurements of Uchida et al. (2002) and the measurements of Seo et al. (2002a) for pores with diameter of 6.0nm. The prediction of this model for the dissociation pressure of CH_4 hydrate is consistent with the former, but is larger than the latter. The data of Uchida et al. (2002) in pores with 30.9nm diameter shows that the P–T condition for hydrate–ice–vapor equilibrium of methane hydrate in narrow pores is the same as that in bulk system, which implies that the interfacial energy between ice phase and hydrate phase equals to zero and the assumption that σ_{HW} equals to σ_{IW} is reasonable.

In many cases, porous media do not have a uniform pore size, but have a pore-size distribution. Putting the pore-size distribution into the model, the P–T condition for H–L–V equilibrium can be calculated by our model. There is no need to modify the model itself. The experimental data reported by Handa and Stupin (1992) and Smith et al. (2002a) represent the isochoric P–T condition for hydrate dissociation in porous media with pore-size distribution. Because the detailed information on pore-size distribution was not given, this study does not try to compare our model with these data. The study of Dicharry et al. (2005) indicates that the isochoric P–T condition for hydrate dissociation can be modeled with Gibbs–Thomson equation and known cumulative volume distribution of the porous media.

Table 2
The molality (mol/kg H_2O) of major ions in 35wt.‰ seawater, in 30wt.‰ oxic seawater and 30wt.‰ euxinic seawater

Ion	35‰ Seawater[a]	30‰ Oxic seawater[b]	30‰ Euxinic seawater[b]
Na^+	0.48559	0.41596	0.44847
K^+	0.01058	0.00880	0.00768
Ca^{2+}	0.01065	0.00918	0.00606
Mg^{2+}	0.05517	0.04732	0.02808
Cl^-	0.56541	0.48492	0.51210
SO_4^{2-}	0.02926	0.02507	0.
HCO_3^-	0.00241	0.00207	0.01515
Br^-	0.00087	0.00073	0.00323
NH_4^+	0.	0.	0.00606

[a] From Riley and Skirrow (1975).
[b] From Dickens and Quinby-Hunt (1997).

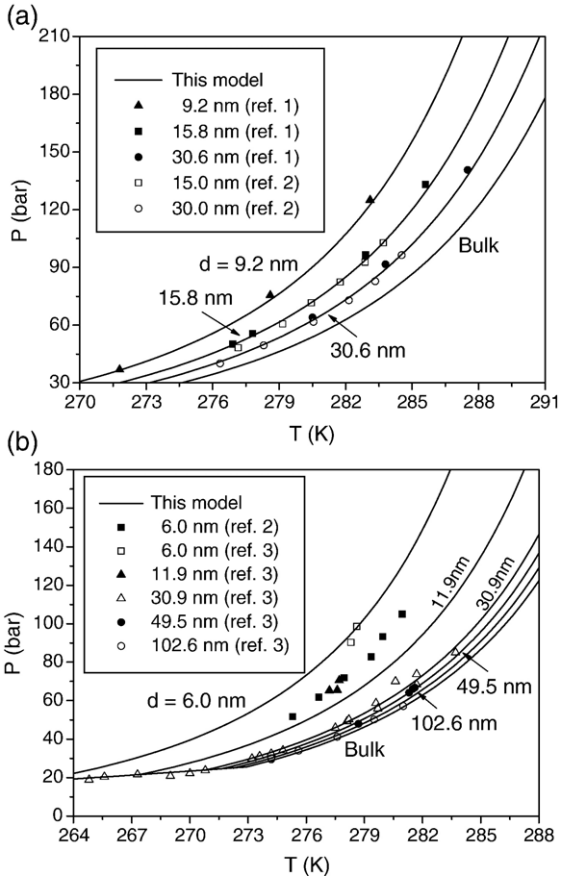

Fig. 3. The prediction of capillary force on H–L–V equilibrium of methane hydrate in the CH_4–H_2O system. The experimental data are from — Ref. 1: Anderson et al. (2003b), Ref. 2: Seo et al. (2002a), Ref. 3: Uchida et al. (2002).

As shown by Fig. 3, capillary force inhibits the formation of methane hydrate. With the decrease of pore sizes, the dissociation (or melting) temperature of methane hydrate will decrease. The inhibition effect of the cylindrical pore with diameter of 32nm equals to the inhibition effect of 35‰ seawater at 283K.

There are few measurements on CH_4 solubility at H–L–V equilibrium, though the data of CH_4 solubility at V–L equilibrium is abundant. Fig. 4 compares the prediction of this model for CH_4 solubility in water at H–L–V equilibrium with the measurements of Servio and Englezos (2002). The agreement between the prediction and experimental data confirms that this model can predict CH_4 solubility at H–L–V equilibrium.

3.2. H–L equilibrium in pure water

There are only a few measurements on CH_4 solubility in liquid phase at H–L equilibrium. These experiments reveal that the CH_4 solubility in liquid in the H–L two-phase region increases with increasing temperature but decreases with increasing pressure, which is opposite to V–L equilibrium. However, there is large discrepancy among the experimental data from the quantitative point of view. For example, the deviation between the two data sets measured by one group (Yang et al., 2001; Kim et al., 2003) is more than 35%.

The prediction of this model for CH_4 solubility in liquid water at H–L equilibrium generally agrees with the experimental measurements. Table 3 gives the average absolute deviations of this model from three experimental data sets. Fig. 5 compares the prediction of this model with some experimental data. In Fig. 5, the lines with positive slope represent CH_4 solubility at H–L equilibrium and the lines with negative slope represent

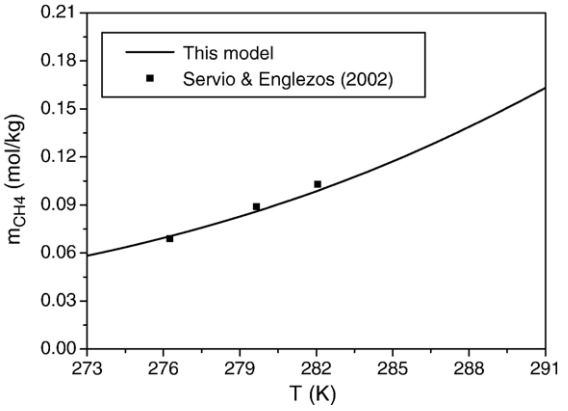

Fig. 4. CH_4 solubility in pure water at H–L–V equilibrium (CH_4 hydrate–liquid water-vapor CH_4 equilibrium): comparison of the prediction of this model with the experimental data.

Table 3
Comparisons of the prediction of this model with experimental CH_4 solubility at H–L equilibrium[a]

Reference	*T* range (K)	*P* range bar)	No. of data	AAD (%)
Seo et al. (2002b)	274–286	60–200	13	8.03
Servio and Englezos (2002)	274–282	35–65	9	2.75
Kim et al. (2003)	276–282	50–144	16	10.42

[a]The data of Yang et al. (2001) are not listed in the Table since it was found erroneous by Kim et al. (2003).

CH_4 solubility at V–L equilibrium. Our predictions for CH_4 solubility in liquid phase at H–L equilibrium agree well with the data published by Servio and Englezos (2002) but are slightly lower than the measurements of Kim et al. (2003). The increasing rate of CH_4 solubility with the increasing temperature of this model agrees with the measurements of Servio and Englezos (2002), and Kim et al. (2003), but is larger than that determined by Seo et al. (2002b). We believe that the prediction of this model and the measurements of Servio and Englezos (2002), and Kim et al. (2003) for CH_4 solubility in water at H–L equilibrium are accurate.

As shown by Fig. 5, CH_4 solubility in liquid increases with the increasing temperature, but will decrease with the increasing pressure. The prediction of the model developed by Zatsepina and Buffett (1997, 1998) is also shown on Fig. 5. It can be found out that the Zatsepina and Buffett's model underestimates CH_4 solubility in liquid at H–L equilibrium. This underestimation resulted from the Trebble–Bishnoi equation of state (Trebble and Bishnoi, 1987, 1988). Hashemi et al. (2006) improved

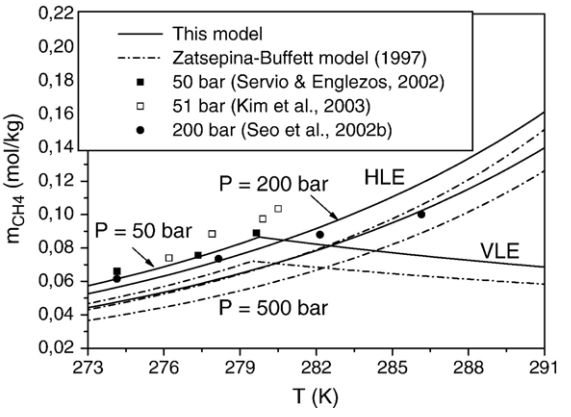

Fig. 5. CH_4 solubility in pure water at H–L equilibrium and at V–L equilibrium: comparison of the prediction of this model with the experimental data. The curves with positive slope represent CH_4 solubility at H–L equilibrium and the curves with negative slope represent CH_4 solubility at V–L equilibrium.

the Trebble–Bishnoi EOS so that the prediction of their model for CH_4 solubility in liquid at H–L equilibrium is as good as our model. However, they did not predict CH_4 solubility in seawater or in aqueous electrolyte solutions.

Seo et al. (2002b) and Huo et al. (2003) measured the cage occupancy ratio θ_L/θ_S (the fraction of the large cages occupied by the guest, θ_L, divided by the fraction of the small cages occupied, θ_S) of methane hydrate at H–L equilibrium via Raman spectroscopy. The discrepancy between the two data sets is relatively big (the large difference of pressure between the two data sets can account for part of the difference of θ_L/θ_S) and the prediction of this model is within the experimental discrepancy (Table 4). The prediction of this model indicates that the occupancy fraction of methane both in small cage and large cage increase with increasing temperature and pressure at H–L equilibrium but the cage occupancy ratio θ_L/θ_S decreases with increasing temperature and pressure.

3.3. H–L equilibrium in seawater and in pore water

Fig. 6 shows that the solubility of methane in liquid at H–L equilibrium decreases with the increase in salinity. Compared to the CH_4–H_2O binary system, CH_4 solubility in 35‰ seawater at H–L equilibrium is reduced by about 10% (e.g. by 8–11% at 200bar from 290 to 273K). Although there is no data available to confirm the prediction of our model for CH_4 solubility in aqueous NaCl solution and in seawater, we believe that our model is accurate since it can predict the salting-out effect of electrolyte on CH_4 solubility with high accuracy at L–V equilibrium.

Based on the fact that salt decreases CH_4 solubility at H–L equilibrium, Zatsepina and Buffett (1998) suggested that the change of salinity provide a positive feedback for hydrate formation. However, they found that this positive feedback occurs only at low salinity. The prediction of their model shows that CH_4 solubility in liquid at H–L equilibrium drops with increasing salinity when the salinity is less than 0.2m of NaCl. At higher salinity, the solubility of methane slowly increases. In contrast, this study found that the solubility of methane at a given P–T condition where methane hydrate is stable decreases with the increase of the molality of NaCl up to 4.7m, suggesting that the positive feedback of salinity changes

Table 4
Comparison the cage occupancy ratio θ_L/θ_S of CH_4 hydrate at H–L equilibrium predicted by this model with the experimental data

Reference	T (K)	P (bar)	θ_L/θ_S(Experiments)	θ_L/θ_S (this model)
Seo et al. (2002b)	274.15	100	1.0534	1.0662
Huo et al. (2003)	275.15	300	1.167±0.04	1.0500

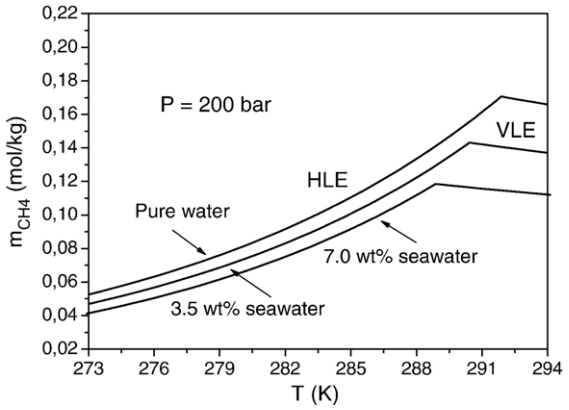

Fig. 6. CH_4 solubility in seawater at H–L equilibrium and at V–L equilibrium. The curves with positive slope represent CH_4 solubility at H–L equilibrium and the curves with negative slope represent CH_4 solubility at V–L equilibrium.

for hydrate formation exists in most of marine environments. The inaccuracy of Zatsepina and Buffett's model arises from the inaccuracy of the activity coefficient model of Aasberg–Petersen (Aasberg-Petersen et al., 1991) as mentioned in Section 2.2.

Methane hydrate generally forms in anoxic sediments. However, the composition of anoxic pore water is significantly different from seawater. Due to ongoing diagenetic progresses, the anoxic pore water is depleted in O_2 and SO_4^{2-}, deficient in Ca^{2+} and Mg^{2+}, enriched in HCO_3^-, NH_4^+ and various trace metals, and elevated in Br^- (Dickens and Quinby-Hunt, 1997; Tishchenko et al., 2005). Tishchenko et al. (2005) tried to predict the difference of CH_4 solubility in seawater and in pore water. Unfortunately, their effort suffered from the absence of the interaction parameters $\lambda_{CH_4-SO_4}$ and $\lambda_{CH_4-HCO_3}$. Duan and Mao (2006) evaluated the interaction parameters between CH_4 and Na^+, K^+, Mg^{2+}, Ca^{2+}, Cl^-, SO_4^{2-}. Here we evaluated the parameters between CH_4 and NH_4^+, HCO_3^-, Br^- (see Appendix B) so that this model can predict CH_4 solubility in pore water. As an example, Table 5 lists some CH_4 solubility data predicted by this model in 30‰ oxic and reductive seawater at H–L equilibrium. The composition of oxic and reductive seawater is taken from Dickens and Quinby-Hunt (1997) and is listed in Table 2. Table 5 indicates that CH_4 solubility in reductive seawater is larger than that in oxic seawater at the same temperature and pressure by about 1.1%.

3.4. Stability of methane hydrate and CH_4 solubility in marine environments

Fig. 7 shows the variation of CH_4 solubility in seawater with pore sizes at H–L equilibrium. The solubility of

Table 5
Comparison of CH_4 solubility in 30 wt.‰ oxic and reductive seawater at H–L equilibrium (the prediction of this model)

T (K)	P (bar)	m_{CH_4} (mol/kg) [a]	m_{CH_4} (mol/kg) [b]
273.15	100	0.05127	0.05184
273.15	300	0.04517	0.04567
283.15	100	0.09587	0.09689
283.15	300	0.08554	0.08648

[a] CH_4 solubility in 30 wt.‰ oxic seawater.
[b] CH_4 solubility in 30 wt.‰ reductive seawater.

methane in water in porous media is greater than that in bulk system for a given temperature and pressure since the capillary force increases the pressure for H–L–V equilibrium in narrow pores and CH_4 solubility at H–L–V equilibrium. CH_4 solubility in liquid at H–L equilibrium increases with the decreasing of pore sizes. The effect of capillary force on CH_4 solubility at H–L equilibrium is opposite to the effect of salts dissolved in water. The smaller the pore sizes, the larger the capillary force and the larger of the CH_4 solubility in liquid water. The increase of CH_4 solubility in small pores with radius less than 18nm can counteract the decrease of CH_4 solubility in 35‰ seawater at 283K and 300bar.

The stability of methane hydrate and methane solubility in liquid within marine sediments is affected by changes in temperature and pressure with depth. As an example, Fig. 8 shows the variation of CH_4 solubility with depth for a typical marine setting (assuming the depth of seawater is 2km, the seafloor temperature is 276.15K, and the geothermal gradient is 40K/km). The pressure in liquid phase equals to the hydrostatic pressure (100bar/km). The base of the hydrate stability zone is marked by a sharp change in the slope of the solubility curves. For example, point A in Fig. 8

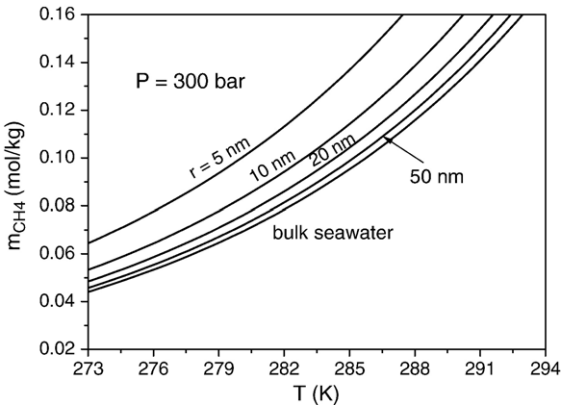

Fig. 7. The variation of CH_4 solubility in seawater at H–L equilibrium with pore sizes.

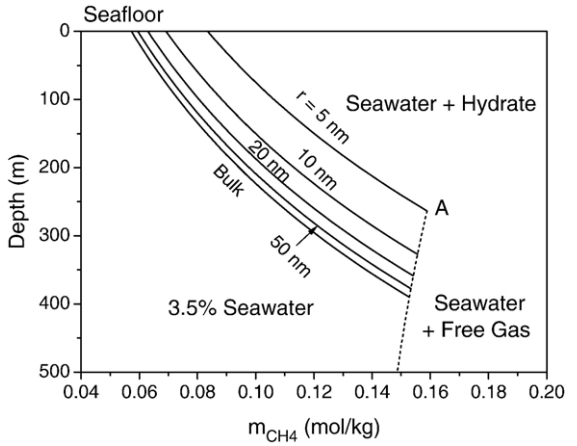

Fig. 8. CH_4 solubility in 35‰ seawater as a function of depth and pore sizes below the seafloor for a typical marine setting. The depth of seawater above the seafloor is 2km. The seafloor temperature is 276.15K, and the geothermal gradient is 40K/km. Pressure is assumed to be hydrostatic (100bar/km).

represents the base of methane hydrate zone in porous sediments with a pore radius of 5nm. The solid lines represent CH_4 solubility in seawater at H–L equilibrium. If methane concentration in seawater exceeds its solubility at the same depth, methane hydrate will form and be stable. In contrast, the dashed line represents CH_4 solubility at V–L equilibrium. If methane concentration exceeds its solubility, free gas phase will form. It can be found out from Fig. 8 that CH_4 concentration needed to form CH_4 hydrate increases with the increase of depth and increases with the decrease of pore size at hydrate stability zone.

A few measurements on host sediments of methane hydrate from ocean drilling or synthetic samples shows that marine sediments bearing CH_4 hydrate have a broad pore-size distribution, ranging from a few nanometers to tens of microns (Clennell et al., 1999; Uchida et al., 2004). The pore-size distribution varies with the composition of the sediments and the degree of consolidation. Fine-grained sediments (e.g. clay, clay-rich silt) have smaller pore size while coarse-grained sediments (e.g. sand, gravel) have larger pore size. The prediction of this model shows that the capillary effect on the P–T condition for H–L–V equilibrium or CH_4 solubility at H–L equilibrium is relatively large for the small pores with radius less than 50nm while the capillary effect is negligible for large pores with radius greater than 500nm. Thus it is necessary to address the capillary effect on the thermodynamic stability of methane hydrates which occur in fine-grained sediments. Our model can calculate the stability of CH_4 hydrate in pore

space with variable size as long as we input the information on the pore size. This study does not try to predict the distribution of methane hydrate in marine sediments since the information on the pore size (the pore-size distribution, the size of pores filled by CH_4 hydrate, and the vertical and horizontal variation of pore size on a regional scale so on) of marine sediments is very limited.

The occurrence of other gas components will shift the *P–T* condition for three-phase equilibrium of methane hydrate. It is known that methane dominates (>99%) the gas in most oceanic gas hydrate but significant C_2H_6, C_3H_8, CO_2 and H_2S occur in samples from some regions (Kvenvolden, 1988, 1995). In general, gas C_2H_6, C_3H_8, CO_2 and H_2S increase the thermodynamic stability of methane hydrate. Based on the experimental data (compiled by Sloan (1998)), adding 1% (mol%) C_2H_6 in coexisting gas phase will decrease the dissociation pressure of CH_4 hydrate by more than 5%. The effect of C_3H_8 is much larger than C_2H_6. Anyway, we should notice that gas analyses were made on the hydrate samples or gas recovered from the core liner for the measurements of gas composition of naturally occurring gas hydrates so that the gas composition reported represents gas composition (excluding H_2O) of hydrate phase, not the composition of coexisting gas phase. Van der Waals–Platteeuw hydrate model implies that C_3H_8, H_2S, C_2H_6, and CO_2 are more enriched than CH_4 in hydrate phase although there is little experimental information on the variation of the composition of mixed hydrate phase with the change of the composition of coexisting gas phase. We estimated that the effect of another gas should be addressed if $z_{C_3H_8}>0.01$, $z_{C_2H_6}>0.02$, $z_{H_2S}>0.02$, or $z_{CO_2}>0.03$ (z_i means H_2O-free mole fraction of gas i in hydrate phase). It is the further work for us to extend this model to multi-component gas hydrates in order to give better prediction of the stability of gas hydrates in marine environments.

4. Conclusion

An accurate thermodynamic model was proposed to predict the stability of methane hydrate in marine environments by taking into account the effect of temperature, pressure, salinity and capillary force together. The chemical potential of hydrate phase is calculated from Van der Waals–Platteeuw hydrate model and angle-dependent ab initio intermolecular potentials as our previous work (Sun and Duan, 2005). Gibbs–Thomson equation with correct parameters for hydrate–water interface is used to account for the capillary effect of porous sediments on H–L–V equilibrium and H–L equilibrium. The effects of the surface textures and mineral components are ignored based on the studies to date. Pitzer model is used to calculate the activity coefficients of H_2O and CH_4 in methane–seawater system. Applying the Poynting correction to calculate the fugacity of methane dissolved in aqueous solution at H–L equilibrium where CH_4 gas does not exist, we extend the model for three-phase equilibrium to two-phase region so that the model can predict CH_4 solubility in aqueous solution at H–L equilibrium.

Comparison of the prediction of this model with experimental data indicates that this model can predict the three-phase equilibrium condition of methane hydrate in seawater and in porous media with high accuracy. Salts dissolved in seawater and the capillary force arising from small pores increase the pressure needed for H–L–V equilibrium for a given temperature. Although there exist only a few experimental data demonstrating the accuracy of the prediction of this model for H–L equilibrium, we believe that this model can reliably predict methane solubility and cage occupancy at H–L equilibrium, since accurate thermodynamic methods are used in this model. The prediction of this model shows that: (1) dissolved salts and the capillary force decrease the *P–T* range for methane hydrate stability; (2) in H–L two-phase region, increasing the salt concentration will decrease the solubility of methane needed to form methane hydrate. The methane solubility will decrease about 10% in 35‰ of seawater; (3) the capillary force increases methane solubility in liquid at H–L equilibrium; (4) within methane hydrate stable zone, CH_4 solubility in liquid increases with depth.

Acknowledgement

This work is supported by Zhenhao Duan's "Key Project Funds" (#40537032) awarded by the National Natural Science Foundation of China, "Major development Funds" (#: kzcx2-yw-124) by Chinese Academy of Sciences, and 973 Project Funds (#2006CB705800) awarded by the Ministry of Science and Technology of China. Thanks to Dr. David Rickard and two anonymous reviewers for their constructive suggestions for the modification of the paper.

Appendix A. The calculation of the Langmuir constants

The Langmuir constant for a guest molecule j in i-type cavity (cage), C_{ij}, is defined as

$$C_{ij}=\frac{Z_{ij}}{kT}=\frac{1}{kT}\int\int \exp\left[-\frac{\Phi(r,\Omega)}{kT}\right]drd\Omega \qquad \text{(A1)}$$

where r is the radial vector of the guest molecule from the center of the cavity, Ω is the orientation vector of the guest molecule in the cavity, Z_{ij} is the full configurational integral, $\Phi(r,\Omega)$ is the total interaction potential between the guest molecule and water molecules surrounding it.

As our previous work (Sun and Duan, 2005), $\Phi(r,\Omega)$ is calculated by using ab initio potential. Since ab initio data are discrete points, we adopted an atomic site–site potential model to fit ab initio potential data. It was proven that this atomic site–site potential model can reproduce the ab initio potential data for CH_4–H_2O and CO_2–H_2O with high quality. The form of the atomic site–site potential model and the list of its parameters are omitted here. The readers can refer to the work of Sun and Duan (2005).

We adopted spherical-cell approximation to estimate the configurational integral Z_{ij} as the work of Anderson et al. (2005). Replacing $\Phi(r,\Omega)$ in Eq. (A1) by spherically averaged potential $W(r)$, we have

$$C_{ij} = \frac{4\pi}{kT}\int_0^{R_{\text{cage}}} \exp\left(\frac{-W(r)}{kT}\right) r^2 dr \qquad \text{(A2)}$$

where R_{cage} means the average radius of the cage. Eq. (A2) can be solved by Simpson integral method with a step of 0.1nm. In order to $W(r)$, we select 576 evenly divided positions on the surface of the sphere with a radius r. For each position, we use 576 orientations for the guest molecules.

Anyway, it is time-consuming to calculate the Langmuir constants according to Eq. (A2). In order to facilitate the application of our model, we try to use a simple formula to fit the Langmuir constants. Eq. (A2) tells us that C_{ij} have the form of exponential function and C_{ij} varies with temperature. After some tries, we select the following empirical equation to fit C_{ij} calculated from Eq. (A2)

$$C_{ij}(T) = \exp(A + B/T) \qquad \text{(A3)}$$

where the unit of T is Kelvin. Table A1 gives the parameters of Eq. (A3) for the Langmuir constants of CH_4 and CO_2 in small and large cages of sI hydrate. The range of temperature of the parameters for CH_4 is from 243K to 318K, and the T range of the parameters for CO_2 is from 253K to 293K. The average absolute deviation between C_{ij} calculated from Eq. (A3) and C_{ij} calculated from Eq. (A2) is less than 0.1%. The maximum deviation is less than 0.2%.

Table A1
The parameters of Eq. (A3) for the Langmuir constants of CH_4 and CO_2 in sI hydrate

Parameter	CH_4 hydrate		CO_2 hydrate	
	Small cage	Large cage	Small cage	Large cage
A	−24.027993	−22.683049	−25.354129	−23.632139
B	3134.7529	3080.3857	3277.0691	3697.1701

Appendix B. The interaction parameters between CH_4 and ions in Pitzer model

In order to calculate the activity of water and the activity coefficient of CH_4 dissolved from Pitzer model (Pitzer, 1991), we need to know the interaction parameters between CH_4 and ions. Duan and Mao (2006) determined the interaction parameters between CH_4 and Na^+, K^+, Mg^{2+}, Ca^{2+}, Cl^-, SO_4^{2-}. This study evaluated the parameters between CH_4 and NH_4^+, HCO_3^-, Br^- from the solubility data of methane in NH_4Cl, $NaHCO_3$, NaBr solutions (Clever and Young, 1987). The results are: $\lambda_{CH_4\text{–}HCO_3}=0.02$, $\lambda_{CH_4\text{–}Br}=0$, $\lambda_{CH_4\text{–}NH_4}=0.7\lambda_{CH_4\text{–}Na}$, and all three-order interaction parameters between CH_4, cation, and anion are approximated to $\zeta_{CH_4\text{–}Na\text{–}Cl}$.

References

Aasberg-Petersen, K., Stenby, E., Fredenslund, A., 1991. Predictions of high-pressure gas solubilities in aqueous mixtures of electrolytes. Ind. Eng. Chem. Res. 30, 2180–2185.

Aladko, E.Y., Dyadin, Y.A., Fenelonov, V.B., Larionov, E.G., Mel'gunov, M.S., Manakov, A.Y., Nesterov, A.N., Zhurko, F.V., 2004. Dissociation conditions of methane hydrate in mesoporous silica gels in wide ranges of pressure and water content. J. Phys. Chem., B 108, 16540–16547.

Anderson, B.J., Bazant, M.Z., Tester, J.W., Trout, B.L., 2005. Application of the cell potential method to predict phase equilibria of multicomponent gas hydrate systems. J. Phys. Chem., B 109, 8153–8163.

Anderson, R., Llamedo, M., Tohidi, B., Burgass, R.W., 2003a. Characteristics of clathrate hydrate equilibria in mesopores and interpretation of experimental data. J. Phys. Chem., B 107, 3500–3506.

Anderson, R., Llamedo, M., Tohidi, B., Burgass, R.W., 2003b. Experimental measurement of methane and carbon dioxide clathrate hydrate equilibria in mesoporous silica. J. Phys. Chem., B 107, 3507–3514.

Ballard, A.L., Sloan, E.D., 2002. The next generation of hydrate prediction I. Hydrate standard states and incorporation of spectroscopy. Fluid Phase Equilib. 194–197, 371–383.

Bogdan, A., 1997. Thermodynamics of the curvature effect on ice surface tension and nucleation theory. J. Chem. Phys. 106, 1921–1929.

Cathles, L.M., Chen, D.F., 2004. A compositional kinetic model of hydrate crystallization and dissolution. J. Geophys. Res. 109, B08102.

Chen, G.-J., Guo, T.-M., 1998. A new approach to gas hydrate modeling. Chem. Eng. J. 71, 145–151.
Clarke, M.A., Pooladi-Darvish, M., Bishnoi, P.R., 1999. A method to predict equilibrium conditions of gas hydrate formation in porous media. Ind. Eng. Chem. Res. 38, 2485–2490.
Clennell, M.B., Hovland, M., Booth, J.S., Henry, P., Winters, W.J., 1999. Formation of natural gas hydrates in marine sediments 1. Conceptual model of gas hydrate growth conditioned by host sediment properties. J. Geophys. Res. 104 (B10), 22985–23003.
Clever, H.L., Young, C.L. (Eds.), 1987. Solubility Data Series, 27/28: Methane. Pergamon Press, Oxford.
Davie, M.K., Zatsepina, O.Y., Buffett, B.A., 2004. Methane solubility in marine hydrate environments. Mar. Geol. 203, 177–184.
Dholabhai, P.D., Englezos, P., Kalogerakis, N., Bishnoi, P.R., 1991. Equilibrium conditions for methane hydrate formation in aqueous mixed electrolyte solutions. Can. J. Chem. Eng. 69, 800–805.
Dicharry, C., Gayet, P., Marion, G., Graciaa, A., Nesterov, A.N., 2005. Modeling heating curve for gas hydrate dissociation in porous media. J. Phys. Chem., B 109, 17205–17211.
Dickens, G.R., 2003. Rethinking the global carbon cycle with a large, dynamic and microbially mediated gas hydrate capacitor. Earth Planet. Sci. Lett. 213, 169–183.
Dickens, G.R., Quinby-Hunt, M.S., 1994. Methane hydrate stability in seawater. Geophys. Res. Lett. 21, 2115–2118.
Dickens, G.R., Quinby-Hunt, M.S., 1997. Methane hydrate stability in pore water: a simple theoretical approach for geophysical applications. J. Geophys. Res. 102 (B1), 773–783.
Duan, Z., Mao, S., 2006. A thermodynamic model for calculating methane solubility, density and gas phase composition of methane-bearing aqueous fluids from 273 to 523K and from 1 to 2000 bar. Geochim. Cosmochim. Acta 70, 3369–3386.
Duan, Z., Sun, R., 2006. A model to predict phase equilibrium of CH_4 and CO_2 clathrate hydrate in aqueous electrolyte solutions. Am. Mineral. 91, 1346–1354.
Duan, Z., Moller, N., Weare, J.H., 1992a. An equation of state for the CH_4–CO_2–H_2O system: I. Pure systems from 0 to 1000 °C and 0 to 8000bar. Geochim. Cosmochim. Acta 56, 2605–2617.
Duan, Z., Moller, N., Greenberg, J., Weare, J.H., 1992b. The prediction of methane solubility in natural waters to high ionic strength from 0 to 250 °C and from 0 to 1600bar. Geochim. Cosmochim. Acta 56, 1451–1460.
Englezos, P., Bishnoi, P.R., 1988. Prediction of gas hydrate formation conditions in aqueous electrolyte solutions. AIChE J. 34, 1718–1721.
Handa, Y.P., 1990. Effect of hydrostatic pressure and salinity on the stability of gas hydrates. J. Phys. Chem. 94 (6), 2652–2657.
Handa, Y.P., Stupin, D., 1992. Thermodynamic properties and dissociation characteristics of methane and propane hydrates in 70-A-Radius silica gel pores. J. Phys. Chem. 96, 8599–8603.
Hardy, S.C., Coriell, S.R., 1973. Surface tension and interface kinetics of ice crystals freezing and melting in sodium chloride solutions. J. Cryst. Growth 20, 292–300.
Hashemi, S., Macchi, A., Bergeron, S., Servio, P., 2006. Prediction of methane and carbon dioxide solubility in water in the presence of hydrate. Fluid Phase Equilib. 246, 131–136.
Henry, P., Thomas, M., Clennell, M.B., 1999. Formation of natural gas hydrates in marine sediments 2. Thermodynamic calculations of stability conditions in porous sediments. J. Geophys. Res. 104 (B10), 23005–23022.
Hillig, W.B., 1998. Measurement of interfacial free energy for ice/water system. J. Cryst. Growth 183, 463–468.
Holder, G.D., Corbin, G., Papadopoulos, K.D., 1980. Thermodynamic and molecular properties of gas hydrates from mixtures containing methane, argon, and krypton. Ind. Eng. Chem. Fundam. 19, 282–286.
Holder, G.D., Mokka, L.P., Warzinski, R.P., 2001. Formation of gas hydrates from single-phase aqueous solutions. Chem. Eng. Sci. 56, 6897–6903.
Huo, Z., Hester, K., Sloan, E.D., Miller, K.T., 2003. Methane hydrate nonstoichiometry and phase diagram. AIChE J. 49, 1300–1306.
Jager, M.D., 2001. High Pressure Studies of Hydrate Phase Inhibition Using Raman Spectroscopy. Ph. D. thesis Thesis, Colorado School of Mines.
Jones, D.R.H., 1973. The measurement of solid–liquid interfacial energies from the shapes of grain-boundary grooves. Philos. Mag. 27, 569–584.
Kim, Y.S., Ryu, S.K., Yang, S.O., Lee, C.S., 2003. Liquid water–hydrate equilibrium measurements and unified predictions of hydrate-containing phase equilibria for methane, ethane, propane, and their mixtures. Ind. Eng. Chem. Res. 42, 2409–2414.
Klauda, J.B., Sandler, S.I., 2001. Modeling gas hydrate phase equilibria in laboratory and natural porous media. Ind. Eng. Chem. Res. 40, 4197–4208.
Klauda, J.B., Sandler, S.I., 2003. Predictions of gas hydrate phase equilibria and amounts in natural sediment porous media. Mar. Pet. Geol. 20, 459–470.
Kleinberg, R.L., Flaum, C., Griffin, D.D., Brewer, P.G., Malby, G.E., Peltzer, E.T., Yesinowski, J.P., 2003. Deep sea NMR: methane hydrate growth habit in porous media and its relationship to hydraulic permeability, deposit accumulation, and submarine slope stability. J. Geophys. Res. 108 (B10) (NO. 2508).
Kvenvolden, K.A., 1988. Methane hydrate—a major reservoir of carbon in the shallow geosphere? Chem. Geol. 71, 41–51.
Kvenvolden, K.A., 1995. A review of the geochemistry of methane in natural gas hydrate. Org. Geochem. 23, 997–1008.
Lee, S.Y., Holder, G.D., 2002. Model for gas hydrate equilibria using a variable reference chemical potential: Part 1. AIChE J. 48, 161–167.
Llamedo, M., Anderson, R., Tohidi, B., 2004. Thermodynamic prediction of clathrate hydrate dissociation conditions in mesoporous media. Am. Mineral. 89, 1264–1270.
Ng, H.-J., Robinson, D.B., 1976. The measurement and prediction of hydrate formation in liquid hydrocarbon–water systems. Ind. Eng. Chem. Fundam. 15, 293–298.
Parrish, W.R., Prausnitz, J.M., 1972. Dissociation pressures of gas hydrates formed by gas mixtures. Ind. Eng. Chem. Process Des. Dev. 11, 26–35.
Pitzer, K.S., 1991. Theory and data correlation. In: Pitzer, K.S. (Ed.), Activity coefficients in electrolyte solutions. CRC Press, London, pp. 75–153.
Prausnitz, J.M., Lichtenthaler, R.N., Gomes de Azevedo, E., 1986. Molecular thermodynamics of fluid-phase equilibria. Prentice-Hall, Englewood Cliffs, N.J.
Riestenberg, D., West, O., Lee, S., McCallum, S., Phelps, T.J., 2003. Sediment surface effects on methane hydrate formation and dissociation. Mar. Geol. 198, 181–190.
Riley, J.P., Skirrow, G., 1975. Chemical Oceanography. Academic Press Inc., New York.
Ruppel, C., 1997. Anomalously cold temperatures observed at the base of the gas hydrate stability zone on the U.S. Atlantic passive margin. Geology 25, 699–702.
Schreiber, A., Ketelsen, I., Findenegg, G.H., 2001. Melting and freezing of water in ordered mesoporous silica materials. Phys. Chem. Chem. Phys. 3, 1185–1195.

Seo, Y., Lee, H., 2003. Hydrate phase equilibria of the ternary CH_4+NaCl+water, CO_2+NaCl+water and CH_4+CO_2+water mixtures in silica gel pores. J. Phys. Chem., B 107, 889–894.

Seo, Y., Lee, H., Uchida, T., 2002a. Methane and carbon dioxide hydrate phase behavior in small porous silica gels: three-phase equilibrium determination and thermodynamic modeling. Langmuir 18, 9164–9170.

Seo, Y., Lee, H., Ryu, B.-J., 2002b. Hydration number and two-phase equilibria of CH_4 hydrate in the deep ocean sediments. Geophys. Res. Lett. 29 (8) (No. 1244).

Servio, P., Englezos, P., 2002. Measurement of dissolved methane in water in equilibrium with its hydrate. J. Chem. Eng. Data 47, 87–90.

Seshadri, K., Wilder, J.W., Smith, D.H., 2001. Measurements of equilibrium pressures and temperatures for propane hydrate in silica gels with different pore-size distributions. J. Phys. Chem., B 105, 2627–2631.

Sloan, E.D., 1998. Clathrate Hydrates of Natural Gases. Marcel Decker, New York.

Smith, D.H., Wilder, J.W., Seshadri, K., 2002a. Methane hydrate equilibria in silica gels with broad pore-size distributions. AIChE J. 48, 393–400.

Smith, D.H., Wilder, J.W., Seshadri, K., 2002b. Thermodynamics of carbon dioxide hydrate formation in media with broad pore-size distributions. Environ. Sci. Technol. 36, 5192–5198.

Sum, A.K., Burruss, R.C., Sloan, E.D., 1997. Measurement of clathrate hydrates via Roman Spectroscopy. J. Phys. Chem., B 101, 7371–7377.

Sun, R., Duan, Z., 2005. Prediction of CH_4 and CO_2 hydrate phase equilibrium and cage occupancy from ab initio intermolecular potentials. Geochim. Cosmochim. Acta 69, 4411–4424.

Sun, R., Huang, Z., Duan, Z., 2003. A new equation of state and Fortran 77 program to calculate vapor–liquid phase equilibria of CH_4–H_2O system at low temperatures. Comput. Geosci. 29, 1291–1299.

Tishchenko, P., Hensen, C., Wallmann, K., Wong, C.S., 2005. Calculation of the stability and solubility of methane hydrate in seawater. Chem. Geol. 219, 37–52.

Tohidi, B., Danesh, A., Todd, A.C., 1995. Modelling single and mixed electrolyte solutions and its applications to gas hydrates. Chem. Eng. Res. Des. 73 (A), 464–472.

Tolman, R.C., 1949. The effect of droplet size on surface tension. J. Chem. Phys. 17, 333–337.

Trebble, M.A., Bishnoi, P.R., 1987. Development of a new four-parameter cubic equation of state. Fluid Phase Equilib. 35, 1–18.

Trebble, M.A., Bishnoi, P.R., 1988. Extension of the Trebble–Bishnoi equation of state to liquid mixtures. Fluid Phase Equilib. 40, 1–21.

Uchida, T., Ebinuma, T., Ishizaki, T., 1999. Dissociation condition measurements of methane hydrate in confined small pores of porous glass. J. Phys. Chem., B 103, 3659–3662.

Uchida, T., Ebinuma, T., Takeya, S., Nagao, J., Narita, H., 2002. Effects of pore sizes on dissociation temperatures and pressures of methane, carbon dioxide, and propane hydrates in porous media. J. Phys. Chem., B 106, 820–826.

Uchida, T., Takeya, S., Chuvilin, E.M., Ohmura, R., Nagao, J., Yakushev, V.S., Istomin, V.A., Minagawa, H., Ebinuma, T., Narita, H., 2004. Decomposition of methane hydrates in sand, sandstone, clays, and glass beads. J. Geophys. Res. 109, B05206.

Van der Waals, J.H., Platteeuw, J.C., 1959. Clathrate solutions. In: Prigogine, I. (Ed.), Advances in Chemical Physics. Interscience, pp. 1–57.

Wilder, J.W., Seshadri, K., Smith, D.H., 2001. Modeling hydrate formation in media with broad pore size distributions. Langmuir 17, 6729–6735.

Xu, W., Germanovich, L.N., 2006. Excess pore pressure resulting from methane hydrate dissociation in marine sediments: a theoretical approach. J. Geophys. Res. 111 (B1) (no. B01104).

Yang, S.O., Cho, S.H., Lee, H., Lee, C.S., 2001. Measurement and prediction of phase equilibria for water+methane in hydrate forming conditions. Fluid Phase Equilib. 185, 53–63.

Zatsepina, O.Y., Buffett, B.A., 1997. Phase equilibrium of gas hydrate: implications for the formation of hydrate in the deep sea floor. Geophys. Res. Lett. 24, 1567–1570.

Zatsepina, O.Y., Buffett, B.A., 1998. Thermodynamic conditions for the stability of gas hydrate in the seafloor. J. Geophys. Res. 103, 24127–24139.

Zhang, Y., Xu, Z., 2003. Kinetics of convective crystal dissolution and melting, with applications to methane hydrate dissolution and dissociation in seawater. Earth Planet. Sci. Lett. 213, 133–148.

Zhang, W., Wilder, J.W., Smith, D.H., 2002. Interpretation of ethane hydrate equilibrium data for porous media involving hydrate–ice equilibria. AIChE J. 48, 2324–2331.

Glossary

a_w	the activity of water
C_{ij}	the Langmuir constant of gas component j in i-type cavity
C_p	isobaric thermal capacity
f_j	the fugacity of gas component j
$f_{CH_4}^{sat}$	the fugacity of CH_4 at P^{sat}
F	the shape factor of solid–liquid interface
h	enthalpy
Δh_w^0	the difference of enthalpy between hydrate phase and ice at 273.15K, =1300J/mol
$\Delta h_w^{\alpha-L}$	the difference of enthalpy between ice and liquid water at 273.15K, =− 6009.5J/mol
$\Delta h_w^{\beta-L}$	the difference of enthalpy between hydrate and liquid water
k	Boltzmann constant, $=1.38 \times 10^{-23}$J/K
m_{CH_4}	CH_4 solubility in liquid
N_A	Avogadro's number, $=6.022 \times 10^{23}$/mol
N_w^β	the number of water molecules per hydrate cell
P	pressure
P^{sat}	the pressure required to obtain a given solubility (x_{CH_4})
r	radius or distance
R	universal gas constant, =8.314J/mol/K
R_{cage}	the average radius of the cage
T	temperature
T_0	the reference temperature, =273.15K
V	molar volume
$\bar{V}_{CH_4}$	the partial molar volume of CH_4 in aqueous solution
$\Delta V_w^{\beta-L}$	the difference of molar volume between hydrate and liquid water
W	spherically averaged total interaction potential between the guest molecule and water molecules
x_{CH_4}	the mole fraction of methane in aqueous solution
Z_{ij}	the full configurational integral
α	the contact angle between the solid phase and the pore wall, radian
γ	activity coefficient
δ	Tolman length
Φ	the total interaction potential between the guest molecule and water molecules
$\zeta_{CH_4-Na-Cl}$	the interaction parameters between CH_4, Na^+, and Cl^-
θ_{ij}	the fractional occupancy of i-type cavities with j-type guest molecules
θ_L	the fractional occupancy of large cavity with methane

θ_S	the fractional occupancy of small cavity with methane
λ_{CH_4-ion}	the interaction parameters between dissolved CH_4 and ion
μ	chemical potential
$\Delta\mu_w^H$	the difference of chemical potential of water between empty hydrate and filled hydrate phase
$\Delta\mu_w^L$	the difference of chemical potential of water between empty hydrate and liquid phase
$\Delta\mu_w^0$	the reference chemical potential difference, = 1202J/mol
v_i	the number of *i*-type cages per water molecule
σ_{ij}	the interfacial energy (interfacial tension) between phase *i* and *j*
σ^∞	the interfacial energy between plane interface

Subscripts

w	water

Superscripts

H	hydrate phase
L	liquid phase
V	vapor phase
α	ice phase
β	hypothetical empty hydrate phase